Chapter 4

Complex Langevin dynamics of spherical dimers

Much of the calibration theory discussed in Chapter 2 assumes that the target particle in question is a single sphere, one who's scattering and motion is easily computed. However, while working with dense colloidal suspensions, one often ends up trapping more than one sphere. Li and Arlt [7] studied the case of two microspheres trapped in a single OT and found that multiple trapped beads could be mistaken for a single trapped bead with altered trap stiffness. Theoretical studies on the case of two trapped microspheres by Xu *et al.* [16] employed a ray-optics based model to show that the two trapped beads are brought into physical contact with each other by optical forces and they also calculated the axial equilibrium positions of the two trapped beads as a function of their size. Experiments in [9] confirmed that the two trapped beads indeed experience different trap stiffnesses in the vicinity of the same potential well. There are further discussions looking into the dynamics of a whole host of asymmetrically shaped particles [3, 8, 14], their results all showing that predicting the behaviour an arbitrary shaped particle comes with great difficulty due to the fact that the optical force is dependent on a greater number of variables such as orientation and size factors.

In this chapter we consider how the addition of a second sphere into an optical trap can radically effect its dynamics, to the extent that one can no longer rely on typical

calibration techniques to characterise the interactions.

4.1 Positional and Orientational dependence of Trapping forces

If we wanted to start from first principles and determine the trap strength on our target particle the first step would be to locate the harmonic traps relative to the trap focus. The methodology for computing optical forces has been covered extensively for a number of different trapping conditions [10], so it is relatively easy to compute the trapping force and determine where a simple sphere would be located relative to focal point of the laser. We can do so because the optical force is only dependent on the particle's relative position. If we instead consider a asymmetric dimer for example we see just by inverting the particle then a secondary harmonic trap can be found below the focus.

We can see that the trap below the focus is comparable in strength to above the focus, however the difference in the transverse strength is far more noticeable. As shown below in Fig **??**, the dimer's orientation and relative position significantly changes the force curve; not only is the trap wider when inverted but the trap stiffness is increased. This highlights one of the challenges involved with studying asymmetric particles, even though its a simple enough process to trap them they maybe characterised very differently depending on their relative position and orientation towards the trap. This can have a significant impact on rheological studies - or attempting to probe any local property - as the variance in trap strength can result in large errors over repeated measurements.

For completeness the harmonic traps were located for dimers across a range of size ratios - from $a_1/a_2 = 1$ to $a_1/a_2 = 10$ - while also recording the trap stiffness for each trap. As a_2 decrease the dimer begins to approximate a single homogenous sphere - at least in terms of location and trap strength. However, for intermediate sized dimers (between $a_1/a_2 = 1.1$ to $a_1/a_2 = 4$), a second harmonic trap appeared below the trapping focus. Previous work using the ray-optics model have confirmed even in the

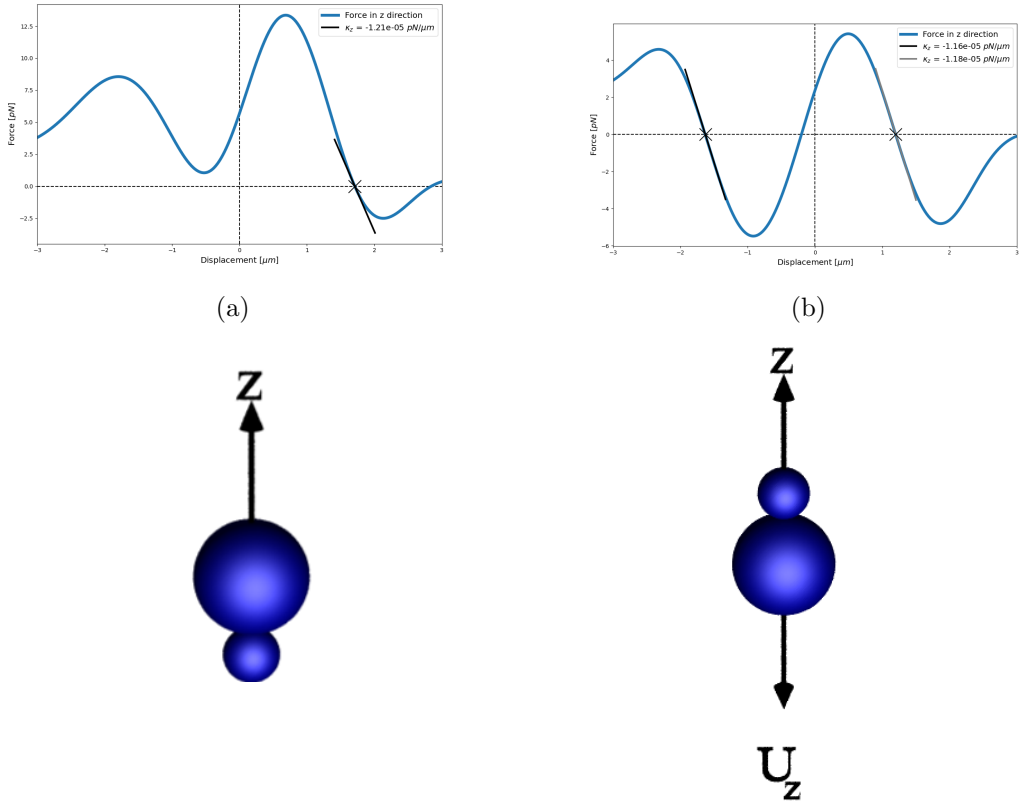

Figure 4.1: Plots of force vs displacement of the point of the contact of the spheres (µm) for the case of a dimer of size ratio 2. (a) is the case where the smaller sphere is orientated with the beam propagation direction. (b) is the inverted case, smaller sphere oriented against the propagation direction. Renders to visualise the dimer orientation are shown below each plot The black lines on each force-curve is a linear fit with the slope being reported as the trap stiffness in the legend.

case that two spheres begin separated the electric field will align the molecules as such that they make contact and are trapped together about a single trapping position [16]. Furthermore it has been shown through proper manipulation of the Gaussian or Bessel beam modes that any number of trapping potentials can be developed [13]. This result however, is the first example of an orientation dependent trapping situation using only a $TEM_0 0$ beam.

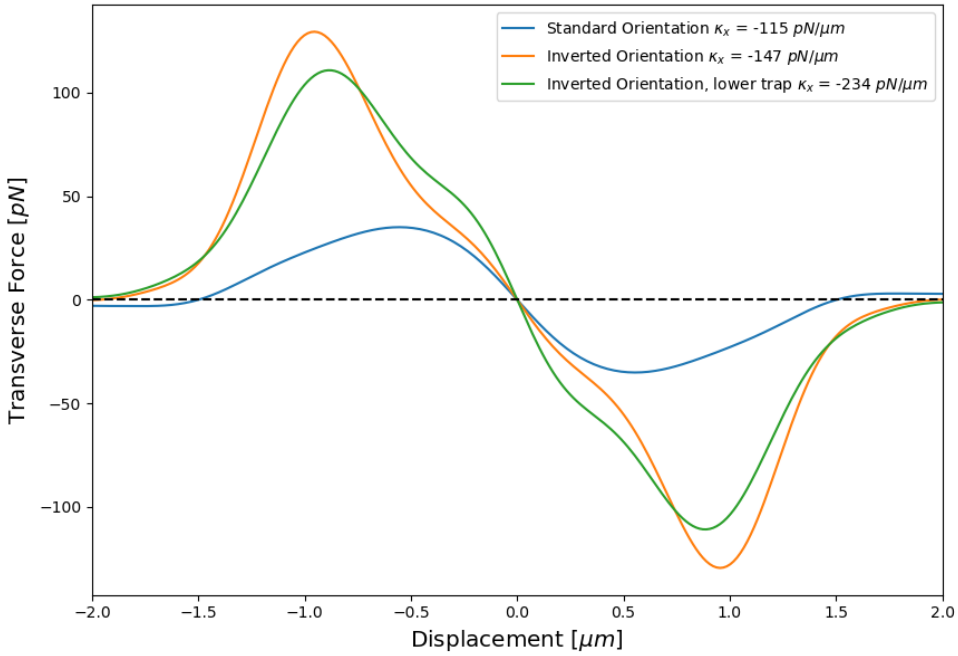

Figure 4.2: Plots of force vs displacement of the point of the contact of the spheres (µm) for the case of a dimer of size ratio 2 while being displaced in the transverse plane. With the blue curve representing the force response for a dimer in its standard orientation, orange being the inverted case, and green the same case but placed below the focus.

4.1.1 Non-trivial harmonic traps

Computing the equilibrium positions when a dimer is aligned with the electric field is relatively simple as the orientational torque is minimised (see Eq.4.1), meaning once trapped the dimer is unlikely to change orientation enough to escape the trap. However, that does not rule out the possibility that there is a stable orientation that is not strictly vertical, in fact most experimental work with symmetric dimers will trap them lying perpendicular to the beam direction [1]. Unlike before where we can simply find the trap by varying the dimer's vertical position its instead more prudent to run a multitude of smaller simulations at a variety of starting positions and orientations. An example for a dimer of size ratio 2 is shown below:

Interestingly while the trap strength of these off-axis traps are similar in magnitude

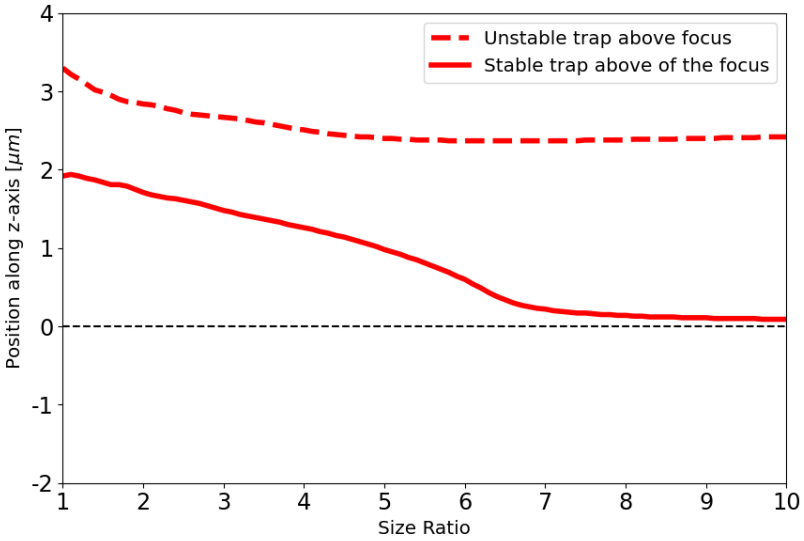

(a)

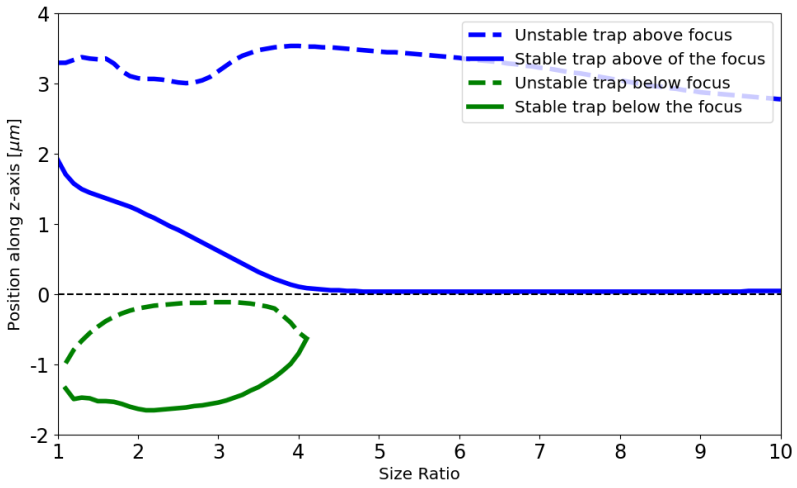

(b)

Figure 4.3: Equilibrium positions of optically trapped dimers with varying size ratio, dotted lines represent unstable traps whereas solid lines represent stable trapping positions. (a) shows that dimers with their smaller sphere orientated away from the focus have an expected single trapping position. (b) shows that when the same dimer is inverted 180° there are now stable traps along the beam axis, one below the focus and one above the focus.

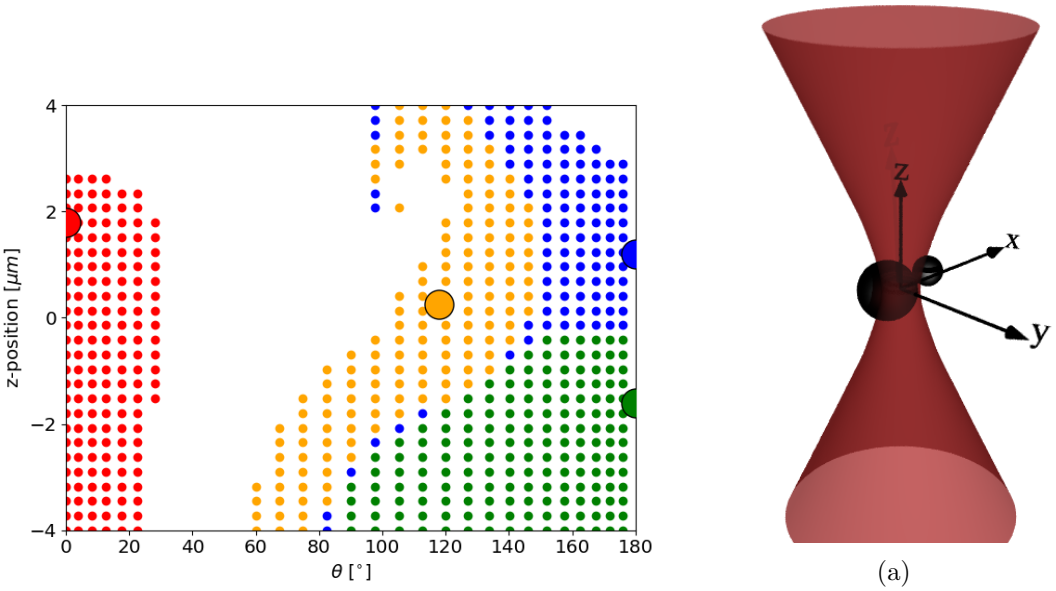

(a)

Figure 4.4: Trajectory map of simulations ran using a dimer of size ratio 2 with a laser power of 500 mW. The stable points are indicated by the larger spheres and the starting conditions are colour coded to match the stable point they end up in. Right hand render shows a dimer in its off-axis configuration

to the vertically aligned dimers, but when the laser power is lowered (around 5 mW) the traps become metastable resulting in the dimer escaping from after some random time while within the trap. If the overall potential depth could be characterised then dimers placed into this orientation could be used as a micro-scale temperature alarm, where by fine tuning of the dimer's parameters would allow you to construct a potential well that can only be escaped when the local fluid temperature exceeds a certain maximum value.

4.2 Continuous rotational motion due to second-order scattering

One aspect that has yet to be covered in depth with regards to spherical aggregates of any construction is their interaction with circularly polarised light. While most homogenous objects are trapped no differently in different polarisations, dimers have been shown to experience an optical torque [1, 12, 15]. Typically the spin density of

an electric field cannot be reduced in homogenous medium due to the fact that the spin angular momentum is conserved locally. In which case the only way to transfer angular momentum to use an object that is anisotropic. This is seen most clearly with birefringent materials, due to fact that the crystal lattice itself is anisotropic, a circularly polarised beam will transfer an optical torque that is proportional to the difference in the refractive index of the particle. The optical torque is given as:

$$\tau_{opt} = \frac{\epsilon}{2\omega_{laser}} E_0^2 (1 - cos(kd(\Delta n)) sin2\phi) \tag{4.1}$$

Where Δn is the difference in refractive indices of the particle, and ϕ indicates the phase shift in the electric field (for circular polarised light $\phi = \pi/4$). The optical rotation seen with dimers can be attributed to the polarisation of the trapping beam as taking a Fourier transform of the transverse components of the dimers orientation time series reveals a clean rotation rate.

A possible explanation of this phenomena was devised by by [17], who found that highly focused Gaussian beams could produce second order effects in the Rayleigh regime resulting in a photo-kinetic force that results in orbital motion about the beam's central axis. This effect is rather minimal for single sphere's, resulting in a orbital frequency on the order of 10^{-1} Hz, with an order of magnitude difference when trapping aggregates of spheres. They computed the circulation rate by computing the time-average probability flux; however, when extended to the Mie regime we see a completely different behaviour, instead experiencing an optical torque about their long axis.S This rotation was first noted by Vigilante and co-workers who only considered this behaviour for a symmetric dimer [15]; we run number of simulations for differently sized dimers in a circularly polarised trap and looked at the rotation rate. We found that not only is the rotation rate dependent on the size of the dimer, but also on its orientation and therefore their axial position.

It is difficult to see from the graph, but the rotation rate never truly goes down to zero, reaching a minimum of 2 Hz, which would imply that a second sphere of radius 200 nm is enough to induce rotational motion. We used *mstm* to look at the stokes

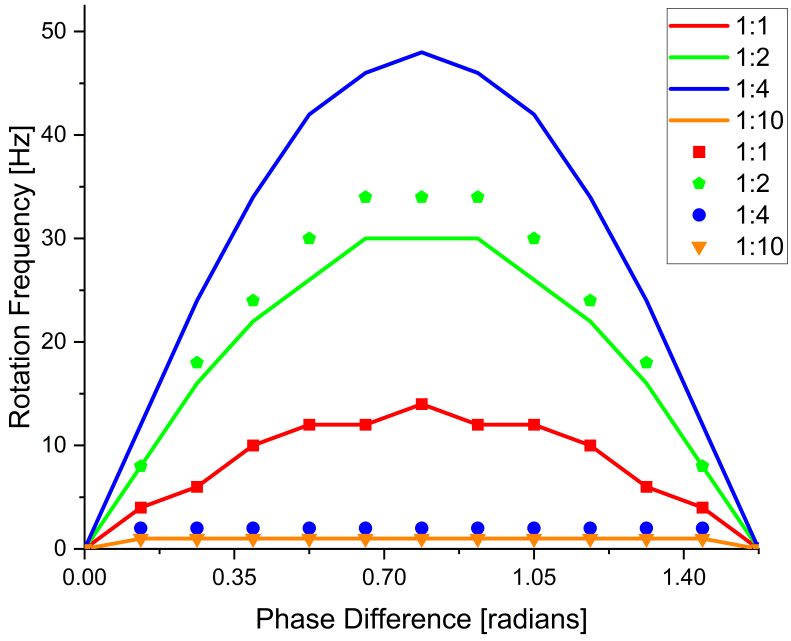

Figure 4.5: Rotation frequency vs component phase difference for differently sized dimers. The solid lines represent the rotation rate experienced while the dimer is in its standard orientation, whereas the solid points are for the case where the orientation is inverted. Laser power = 100 mW

parameters from the scattered field from a simple plane wave incident on our dimer, the proportion of circularly polarised light is minimal compared to the proportion of plane polarised light, which indicates that this rotational motion is not due to any inhomogeneity in the dimer that might impart angular momentum to the scattered beam - as compared to a anisotropic scatterer like vaterite.

These results are somewhat contrary to other work with silica dimers [1, 4, 12]; previous experiments have trapped the dimer in an orientation perpendicular to the beam propagation direction. The rotational motion is induced due to the asymmetric geometry creating an unbalanced polarisation susceptibility along its long axis as compared to its short axis; therefore its long axis is aligned with the polarisation vector and can rotate freely [1]. This however cannot be the case with our simulations as the dimer rotates about its long axis, meaning there cannot be an asymmetric axis to align with the

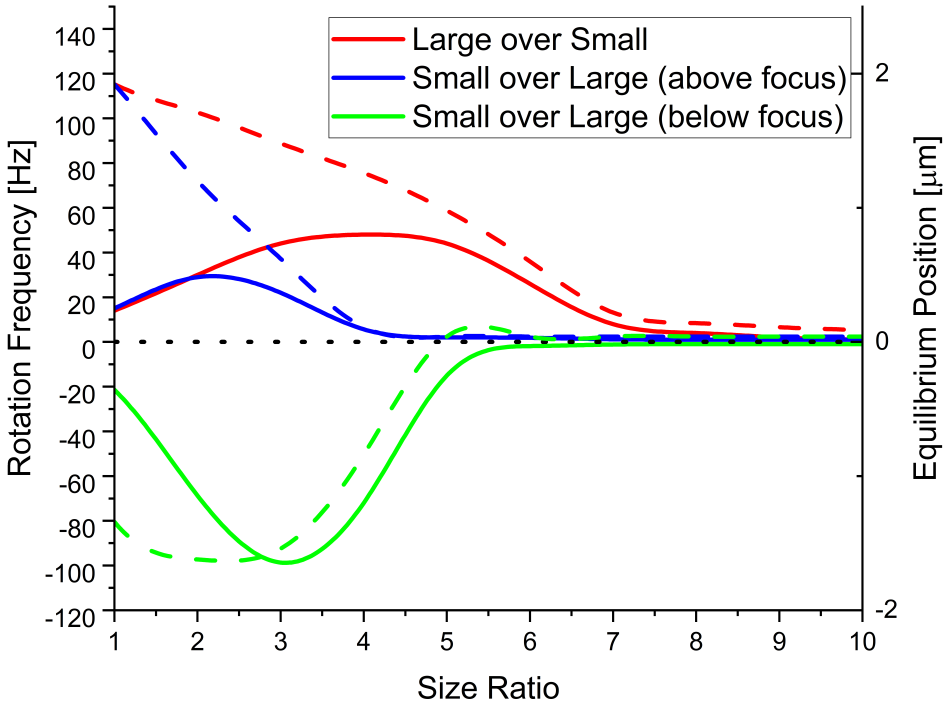

Figure 4.6: Rotation rate plotted against dimer size ratio for a variety of different simulation scenarios. The red line is for the case where the larger sphere is above the smaller sphere. The blue line is the inverted case, while the initial position is above the focus of the trap. And lastly the green line is again for the inverted case, but when the dimer's initial position is below the focus of the trap.

beam's polarisation vector. Furthermore, we see a non-linear increase in the rotational speed of our dimers with size, the drag torque from the surrounding fluid is $\propto r^3$ so the expectation is that the rotation frequency should fall off with increasing size. This indicates that the rotational motion is due to the shape asymmetry of the dimer and not solely due to the beam's angular momentum. Measurement of this photo-kinetic force is difficult to achieve due to the fact that previous analysis was conducted in the Rayleigh regime, where the polarizability of our dimer can be approximated as:

$$\mathbf{p}(\mathbf{r},t) = \alpha_x E_x(\mathbf{r},t)\hat{\mathbf{e}}_x + \alpha_y E_y(\mathbf{r},t)\hat{\mathbf{e}}_y + \alpha_z E_z(\mathbf{r},t)\hat{\mathbf{e}}_z \tag{4.2}$$

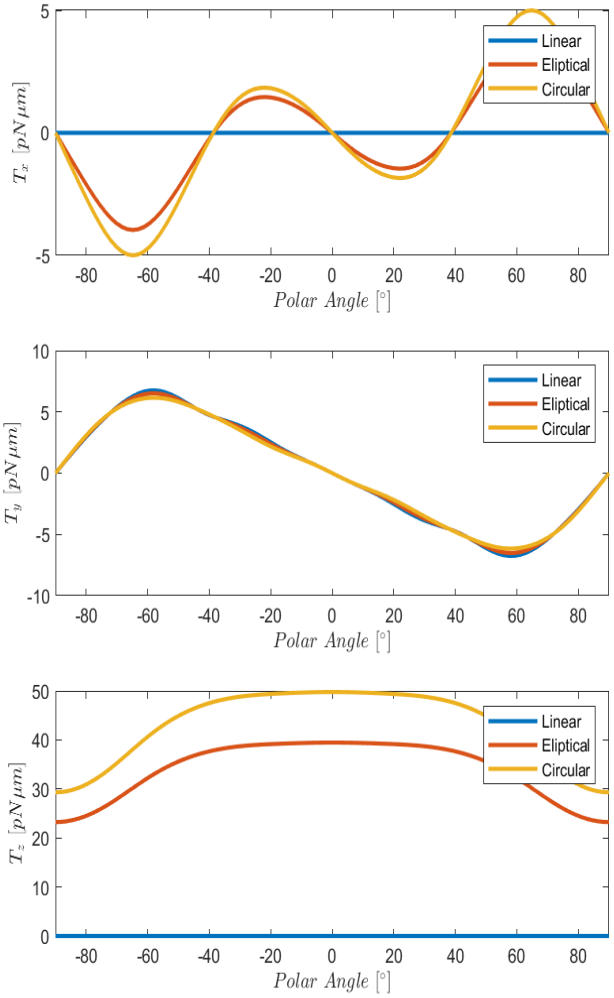

Figure 4.7: Optical torque against polar angle θ about the three primary axis (top: torque about the x-axis; middle: torque about the y-axis; bottom: torque about the z-axis) on a symmetric dimer in linear, elliptical, and circular polarisation beams. Diagram to the right is for visual clarity about the direction of θ.

where the polarizability is given as a 3D vector for the three principle Cartesian directions. In order to measure the magnitude of second order contributions we would need to construct a dipole array that fully captures the scattering of a dimer. Measuring the optical torque makes it clear that the polarizability is a contributing factor to this optical rotation phenomena. Rotating a symmetric dimer in the $x-z$ plane reveals that while the dimer can be rotated in an orientation perpendicular to the beam rotational torque is maximised when rotated while aligned with the optical axis.

4.2.1 Gyroscopic Precession using asymmetric dimers

As mentioned in section 4.1.1 for specificity sized dimers there is the potential for non-vertical trapping orientations in which the dimer is located in a harmonic trap. When trapped by a circularly polarised light these dimers exhibit gyroscopic precession. As shown in fig **??** the dimer's is rotating about it's long axis (as seen by the periodic behaviour of u_x and u_y), while also precessing around the optical axis of the beam, resulting in a second order oscillation in s_z.

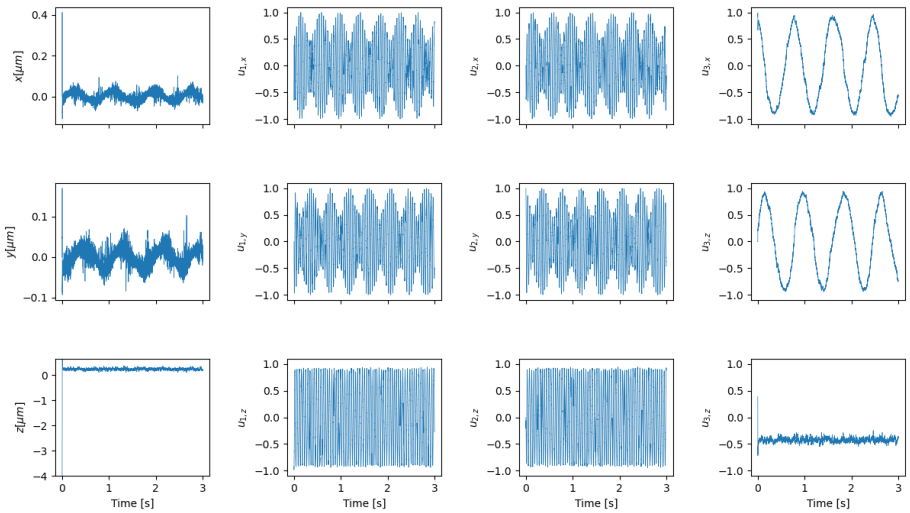

Figure 4.8: 3 second trajectory of a dimer trapped in an off axis orientation, laser power was set to 100 mW. The far left column depicts the dimer's centre of mass position with time; middle two columns are the x, y, and z components of the vectors u_x and u_y; last column depicts the components of the vector u_z which defines the dimer's orientation.

Applying a Fourier analysis to the above trajectory reveals the 3 fundamental frequencies typically associated with precession; the $u_{z,1}$ and $x(t)$ series show a precession frequency of $1.33\ Hz$ whereas the series $u_{x,1}$ and $u_{y,1}$ show a combined periodic signal - a rotational frequency of $23\ Hz$ and a nutation frequency of $20\ Hz$. Previous studies into amorphous silica nanoparticles found a linear relationship with the rotational frequency and the laser power, but no such relationship existed with the precession frequency. Our own results shows a similar linear relationship with vertically aligned

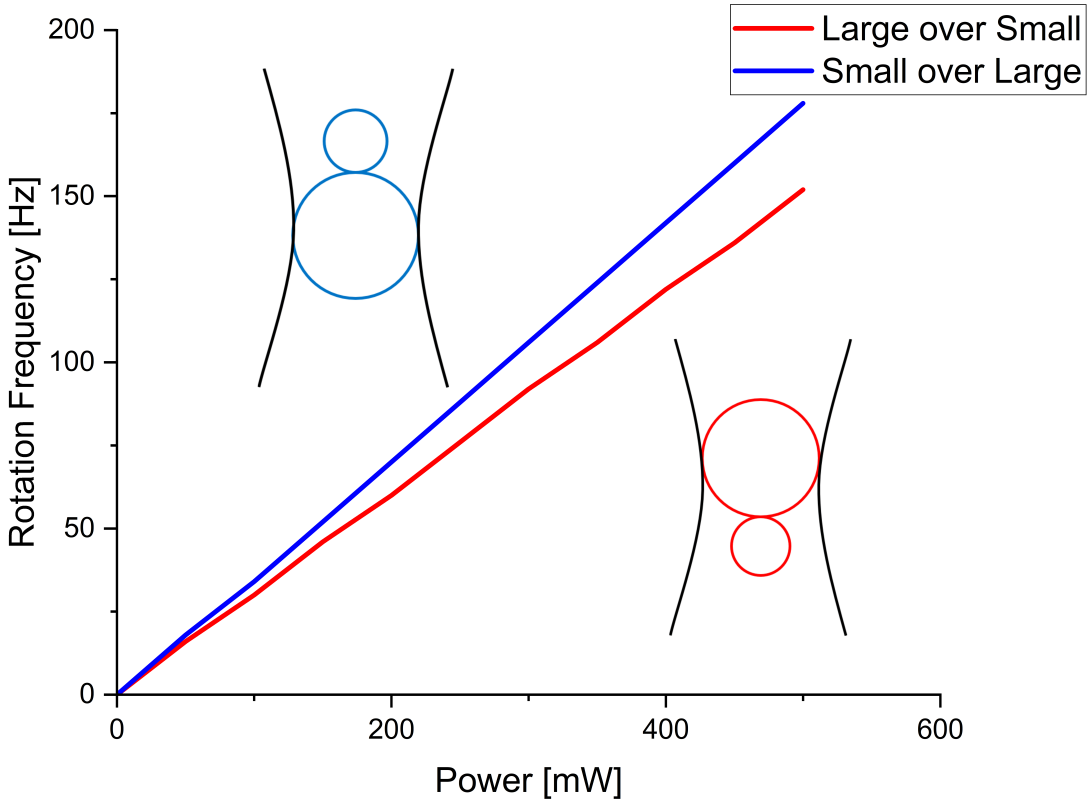

Figure 4.9: Rotational frequency vs laser power for a dimer in both vertical orientations.

dimers.

The linear relationship could partly be due to fact that we do not account for the change in viscous forces with increasing laser power. It is far more likely that the rotational frequency reaches a maximum value assuming that the bulk fluid can readily absorb the laser.

This gyroscopic motion has been demonstrated previously in nanoparticles [5, 6, 11, 18] but has not been observed for micron scale aggregates. Since the torque is computed by evaluating the beam coefficients it is be difficult to apply this result to micro-rheology experiments as one would need to know the exact magnitude of the optical torque ahead of time in order to make estimations about the local fluid viscosity. This is trivial for a birefringent spherical particle, less so for spherical aggregates whose equilibrium position and orientation are unknown.

4.3 Characterisation of asymmetric dimers via PSD analysis

As discussed in **??**, one of the methods developed to work in conjunction with [15] is a simulated quadrant photo diode for as a position detection system. While it is possible to extract all of the relevant dynamical information from a simulation, confirming the same behaviour in an experimental setting can be challenging.

As a benchmark we start by considering a single sphere within an optical trap. After a 3 second trajectory (the typical time necessary to collect a power spectrum) the sphere's power spectra was recorded and a fitted to eq. **??**.

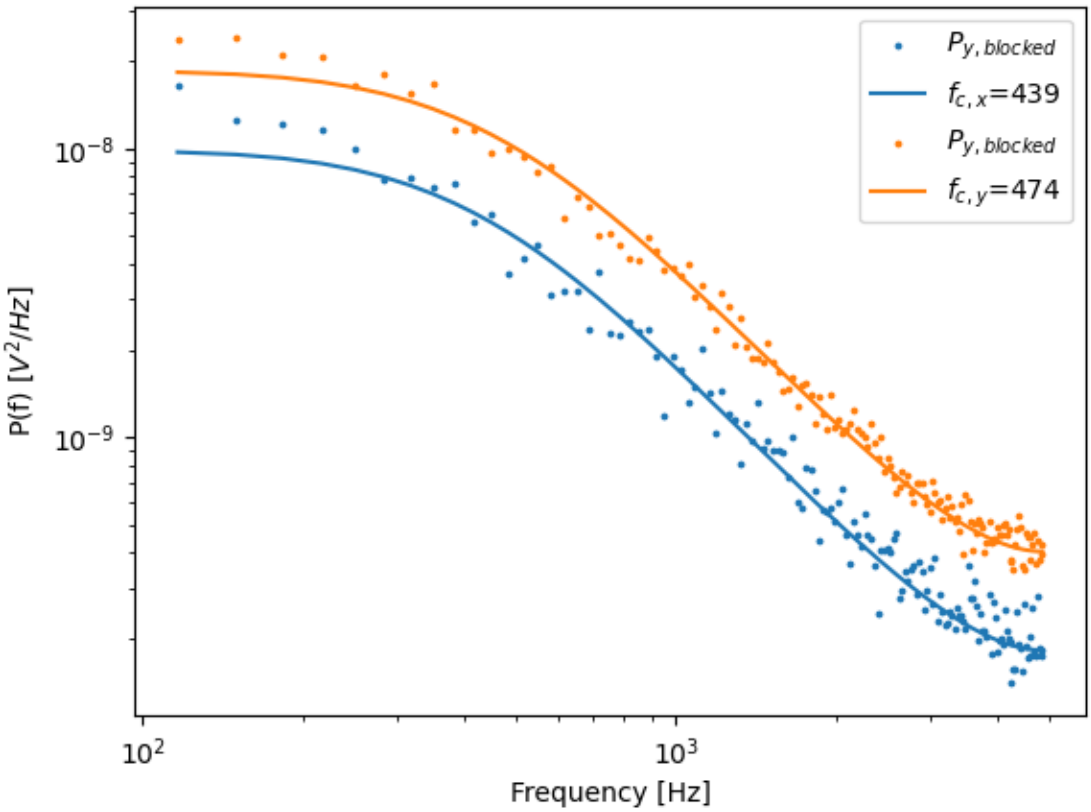

Figure 4.10: Recorded power spectra fitted to eq. **??**, scattered points represents the blocked data ($n_b = 100$). Corner frequency for the Lorentzian curves are reported in the legend.

As shown in fig. **??**, the two power spectra report different corner frequencies which

would be indicate that the trap is not perfectly circular. Using *ott* we can compare the expected trap strength to what is reported by a quadrant photo diode:

Fitting parameter	*ott* estimates		QPD fitting		Simulation fitting	
f_c $[Hz]$	447	450	439	474	523	513
κ $[pN/\mu m]$	53.05	53.40	51.96	56.09	61.94	60.7
Ellipticity	8.16 %		27.17 %		13.8 %	

Where the ellipticity of the beam is given by $e = (1 - \kappa_y/\kappa_x)^{0.5}$ and is a measure of the symmetry of the beam wavefront. Its clear from these initial results that the QPD is more sensitive to changes along the y-axis than the x-axis when compared to the direct *ott* calculations. Typically, even an industrial Gaussian beam will produce an elliptical diffraction limit spot when heavily focused; in their tutorial for optimizing the PSD analysis, Berg and Sorensen reported a ellipticity of around 15 % after a total calibration time of 81 seconds [2]. The reason for this discrepancy can be explained partly by the fact that our estimation of the trap geometry via *ott* is based on the force-displacement curve while the sphere is moving in only one direction, whereas the QPD is estimating the trap geometry by extrapolating from far field scattering signals. We now consider a symmetric dimer in identical simulative conditions.

Fitting parameter	*ott* estimate		QPD fitting		Simulation fitting	
f_c $[Hz]$	409	334	431	424	274	285
κ $[pN/\mu m]$	48.51	39.58	51.13	50.26	32.45	33.75
Ellipticity	42.8 %		12.7 %		13.8 %	

Now we see that the *ott* predicts a more elliptical trap compared to the QPD model which says the trap is far more symmetrical while trapping a symmetric dimer. A potential reason that *ott* no longer expects a circular trap could be due to how it computes the beam shape coefficients; by point matching in the far field before the focus means a loss in accuracy for objects that trap above the focus. The change in the QPD estimation can be partially explained by the fact that rotational effects are not accounted for in the Lorentzian power spectra, only translational motion. Typically, rotational motion is only ever detected when it is periodic (take for example Fig. **??**), when the

motion is stochastic the entire power spectra is effected making it near impossible to separate the translational and rotational contributions from a single power spectra.

4.4 Conclusions

Considering the simplicity of a scatterer such as a dimer, one would assume that the dynamics of such an object would be relatively easy to predict. Simulations of dimers in the Mie regime show that not only do they have multiple positions and orientations in which they can be trapped but also that their interaction with circularly polarised light is heavily dependent on the axial position and trapping orientation. Dimer's have the potential to be used as adaptive micro-rotors, being simple to synthesise and can be made out of any material of choice, but in order for these particles to be used as such one needs a means of characterising the optical torque applied. While estimations can be made in the Rayleigh regime due to the dimer being treated as point dipole, Mie regime micro rotors require an in-depth theoretical description of the mechanism that is creating this optical torque.

Bibliography

[1] J. Ahn, Z. Xu, J. Bang, Y.-H. Deng, T. M. Hoang, Q. Han, R.-M. Ma, and T. Li. Optically levitated nanodumbbell torsion balance and ghz nanomechanical rotor. *Physical Review Letters*, 121(3):033603, July 2018.

[2] K. Berg-Sørensen and H. Flyvbjerg. Power spectrum analysis for optical tweezers. 75:594–612, 2004.

[3] C. D, P. P, N. B V, S. Bhattacharya, and S. Ananthamurthy. Laser polarization driven micromanipulation and reorientation dynamics of an asymmetric shaped microscopic biomaterial using optical tweezers. *Journal of Optics*, 24(9):094007, Aug. 2022.

[4] R. Debuysschère, B. Rimez, A. Zaccone, and B. Scheid. Experimental and theoretical investigation of nonclassical shear-induced nucleation mechanism for small molecule. *Crystal Growth & Design*, 23(7):4979–4989, June 2023.

[5] T. M. Hoang, Y. Ma, J. Ahn, J. Bang, F. Robicheaux, Z.-Q. Yin, and T. Li. Torsional optomechanics of a levitated nonspherical nanoparticle. *Physical Review Letters*, 117(12):123604, Sept. 2016.

[6] S. Kuhn, A. Kosloff, B. A. Stickler, F. Patolsky, K. Hornberger, M. Arndt, and J. Millen. Full rotational control of levitated silicon nanorods. 2016.

[7] M. Li and J. Arlt. Trapping multiple particles in single optical tweezers. 281:135–140, 2008.

[8] J. C. Loudet, B. M. Mihiretie, and B. Pouligny. Optically driven oscillations of ellipsoidal particles. part ii: Ray-optics calculations. 37, 2014.

[9] P. Praveen, Yogesha, S. S. Iyengar, S. Bhattacharya, and S. Ananthamurthy. Two particle tracking and detection in a single gaussian beam optical trap. 55:585, 2016.

[10] A. A. Ranha Neves and C. L. Cesar. Analytical calculation of optical forces on spherical particles in optical tweezers: tutorial. *Journal of the Optical Society of America B*, 36(6):1525, May 2019.

[11] M. Rashid, M. Toroš, A. Setter, and H. Ulbricht. Precession motion in levitated optomechanics. *Physical Review Letters*, 121(25):253601, Dec. 2018.

[12] R. Reimann, M. Doderer, E. Hebestreit, R. Diehl, M. Frimmer, D. Windey, F. Tebbenjohanns, and L. Novotny. Ghz rotation of an optically trapped nanoparticle in vacuum. *Physical Review Letters*, 121(3):033602, July 2018.

[13] V. Shahabadi and E. Madadi. Effective multiple optical trapping of sub-micrometer particles with petal beams. *Journal of the Optical Society of America B*, 37(12):3665, Nov. 2020.

[14] X. Sheng-Hua, L. Yin-Mei, L. Li-Ren, and S. Zhi-Wei. Computer simulation of the collision frequency of two particles in optical tweezers. 14:382–385, 2005.

[15] W. Vigilante, O. Lopez, and J. Fung. Brownian dynamics simulations of sphere clusters in optical tweezers. *Optics Express*, 28(24):36131, Nov 2020.

[16] S. Xu, Y. Li, and L. Lou. Axial optical trapping forces on two particles trapped simultaneously by optical tweezers. 44:2667, 2005.

[17] A. Yevick, D. J. Evans, and D. G. Grier. Photokinetic analysis of the forces and torques exerted by optical tweezers carrying angular momentum. *Philosophical Transactions of the Royal Society A: Mathematical, Physical and Engineering Sciences*, 375(2087):20150432, Feb. 2017.

[18] Q. Zhu, N. Li, H. Su, W. Li, and H. Hu. Dynamic analysis and simulation of an optically levitated rotating ellipsoid rotor in liquid medium. *Photonic Sensors*, 12(2):105–116, Sept. 2021.